Deletion of Bak1 alleviates microglial necroptosis and neuroinflammation after experimental subarachnoid hemorrhage

Xiancheng Qiu
the Affiliated Hospital of Southwest Medical University
Qianke Tao
the Affiliated Hospital of Southwest Medical University
Lihan Zhang
the Affiliated Hospital of Southwest Medical University
Chenghao Kuang
the Affiliated Hospital of Southwest Medical University
Yuke Xie
the Affiliated Hospital of Southwest Medical University
Lifang Zhang
the Affiliated Hospital of Southwest Medical University
Shigang Yin
Southwest Medical University
Jianhua Peng (pengjianhua@swmu.edu.cn)
the Affiliated Hospital of Southwest Medical University
Yong Jiang
the Affiliated Hospital of Southwest Medical University

Research Article

Keywords: Subarachnoid hemorrhage, Microglia, Necroptosis, Neuroinflammation, Bak1

Posted Date: May 10th, 2022

DOI: https://doi.org/10.21203/rs.3.rs-1515494/v2

Abstract

Background

Microglial necroptosis exacerbates neurodegenerative diseases, central nervous system injury and demonstrates a pro-inflammatory process, but its contribution to subarachnoid hemorrhage (SAH) is poorly characterized. BCL-2 homologous antagonist-killer protein (Bak1), a critical regulatory molecule of endogenous apoptosis, can be involved in the pathological process of necroptosis by regulating mitochondrial permeability. Despite its possible significance in microglia necroptosis-mediated inflammation, few studies have investigated Bak1's role in microglia necroptosis regulation.

Methods

In vivo, an experimental subarachnoid hemorrhage in mice identified microglia necroptosis and adeno-associated virus targeted interference with microglia Bak1 to determine its effect on neuroinflammation. In vitro knockout of Bak1 in BV2 microglia identified its regulatory role in microglia necroptosis and neuroinflammation, and RNA-Seq clarified the potential downstream regulatory mechanisms.

Results

Microglia undergo necroptosis after subarachnoid hemorrhage in vivo and vitro. Knocked-down of Bak1 by adeno-associated virus attenuates microglial necroptosis, alleviates neuroinflammation, and improves neurological function after SAH. Increasing Bak1 expression and mediating BV2 microglia pro-inflammatory phenotype transformation, exacerbating oxidative stress and neuroinflammation. Abrogating Bak1 reduces necroptosis by downregulating the expression of phosphorylated pseudokinase mixed lineage kinase domain-like protein (p-MLKL), then downregulating pro-inflammatory phenotype gene expression. RNA-Seq shows that disrupting BV2 Bak1 downregulates multiple immune and inflammatory pathways and ameliorates cell injury by elevating Thrombospondin 1 (THBS1) expression.

Conclusions

Our finding demonstrated that deletion of bak1 alleviates microglial necroptosis, neuroinflammation and improved neurological functions after SAH, which was, at least in part, mediated by activation of THBS1 signaling pathway. Bak1 may be a potential therapeutic strategy for the management of SAH.

Introduction

Subarachnoid hemorrhage (SAH) is a severe subtype of stroke produced mainly by intracranial artery rupture with high mortality and fatality rates. Despite massive efforts worldwide, Challenges remain to relate to early management and long-term outcomes of SAH. Early neuroinflammation following SAH is

one of the top courses for poor prognosis, while clinical trials have failed to provide consistent evidence for the use of anti-inflammatory agents in SAH patients. Thus, it's crucial to provide insight into its pathogenic mechanisms and develop innovative therapeutic strategies for SAH patients [1, 2].

Cell necrosis promotes neurological deficits and exacerbates brain injury following subarachnoid hemorrhage by eliciting a severe pro-inflammatory response, as opposed to apoptosis, which is typically considered to be immunosilent. Recent research shows regulable necrosis subtypes, including ferroptosis, pyroptosis, and necroptosis, and demonstrates a detrimental role for these programmed cell deaths during early brain injury following subarachnoid hemorrhage[3–5]. These forms of cell death have morphological features with necrosis, such as membrane rupture, organelle swelling, and release of cell contents; their molecular regulatory mechanisms are distinct and are intimately related to the inflammatory response[6]. Among them, necroptosis is triggered by the Receptor-interacting serine/threonine-protein kinase 1 (RIPK1), Receptor-interacting serine/threonine-protein kinase 3 (RIPK3), Mixed lineage kinase domain-like protein (MLKL) cascade reaction, resulting in the release of damage-associated molecular patterns (DAMPs) and ultimately resulting in inflammation[7, 8].

BCL-2 Homologous Antagonist-Killer Protein (Bak1), a mitochondrial apoptosis effector molecule in the BCL-2 protein family, has recently emerged to play a vital role in regulating pyroptosis, and activation of Bak1 inhibits IAP proteins promoting caspase-8-mediated activation of Interleukin-1 beta (IL-1β) and inducing NLRP3 inflammasome-mediated caspase-1-dependent IL-1β maturation, Promotes pyroptosis and aggravates inflammatory response[9]. Additionally, it has been demonstrated that Bak1 plays a critical function in the regulation of mitochondrial outer membrane permeability (MOMP) downstream of necroptosis and enhances Mitochondrial Permeability Transition Pore (MPTP)-dependent necrosis[10]. However, the precise mechanism by which Bak1 contributes to the inflammatory response in SAH necroptosis remains unknown, and additional investigation is required to elucidate.

In this study, we explored the regulatory mechanisms of Bak1 in the necroptosis and neuroinflammation of microglia in experimental subarachnoid hemorrhage. We found that the knockout of Bak1 down-regulated the phosphorylated pseudokinase mixed lineage kinase domain-like protein (p-MLKL) content alleviated the necroptosis and pro-inflammatory phenotype of microglia, and reduced neuroinflammation. RNA-Seq verified the potential mechanism of Bak1 regulating necroptosis, and it was determined that Bak1 could reduce the inflammatory response and cell injury by elevating Thrombospondin-1 (THBS1), providing a new concept and therapeutic strategy for the treatment of neuroinflammation after subarachnoid hemorrhage.

Materials And Method

Animals

C57BL/6J male healthy mice (8-12 weeks old, average weight 18-22g) were accommodated in the IVC animal husbandry system of the Medical Animal Center of the Affiliated Hospital of Southwest Medical University, where the ventilation system and internal hygiene of the cages were kept in good condition, the

humidity inside the cages was controlled at 55%-65%. The constant temperature inside the cages was maintained at 24-25°C. The animals were exposed to a 12-hour cycle of light, were protected from light, and rested quietly at night. The animals all have free access to fresh feed and drinking water.

Animal experimental design

Experiment 1. To examine the changes of RIPK1/RIPK3 during early brain injury in subarachnoid hemorrhage, Mice used for protein abundance assay were divided into four groups: Sham (n=5), SAH 24h (n=5), SAH 48h (n=5), SAH 72h (n=5), and the injured lateral hemispheres were harvested after modeling for subsequent validation. Immunofluorescence staining was used to determine the co-localization of MLKL with microglia in the 24h group (N=6), Pyridinium iodide staining to detect cell necrosis and to detect co-localization with microglia (N=6).

Experiment 2. Targeted knockdown of mice microglia Bak1 protein using pAAV-CD68p-Bak1-shRNA adeno-associated virus (shanghai genechem Co., Ltd. CN). Bak1 target sequence is 5'-GCTCTCATCGGAGATGATATT-3', NC negative control sequence is 5'-TTCTCCCCGAACGTGTCACGT-3'. Mice were injected with the adeno-associated virus in the lateral ventricle for 3ul and then monitored for viral expression for three weeks. Different C57BL/6J male mice groups were randomly selected after infection for subsequent experimental validation. WB detection of RIPK1, RIPK3 expression in the ipsilateral cerebral hemisphere 24h after SAH molding, NC group (n=5), Bak1-KD (N=5), ELISA for pro-inflammatory factor concentration (IL-6, IL-1β, TNFα), NC group (n=5), Bak1-KD (n=5). Co-localization of PI and microglia IBA1 were detected by immunofluorescence, NC group (n=3), and Bak1-KD group (n=3).

Subarachnoid hemorrhage model

Induction of SAH model by modified single-clamp puncture method[11]. The primary process is: Anesthesia was induced in experimental mice with 4-5% isoflurane, followed by intraperitoneal injection of 1% pentobarbital sodium to create continuous anesthesia. The mice were placed supine on the operating table with a satisfactory level of anesthesia (no significant pain from skin incision). After skin preparation and disinfection, the skin of the neck was incised along the anterior midline of the neck using a sharp surgical blade (an incision of approximately 1 cm in length was sufficient). Micro forceps bluntly separated the subcutaneous fat, deep fascia, and muscle tissue, preserved the hyoid bone, pulled the hyoid bone to the side, exposed the right common carotid artery, separated the vessels and peripheral nerves, and then freed the right external carotid artery, down and on its serious side, separated the right internal carotid artery. After resistance is felt at the bifurcation of the anterior and middle cerebral arteries, the puncture wire is advanced 2mm further through the vessel and immediately returned. We also observed whether the mice showed typical Cushing's reaction, which was used as an indirect criterion to judge the success of the SAH model. After the puncture is completed, the puncture wire is quickly withdrawn. The blind end of the external carotid artery vessel is ligated, the skin incision is sutured, and the skin is disinfected with dilute iodophor. Mice in the Sham group were performed the same surgical procedure. Still, instead of puncturing the vessel, the puncture line was immediately returned after resistance was felt at the bifurcation of the anterior and middle cerebral arteries. The mice were placed in

a rewarming chamber at 25°C and observed and recorded every 15 minutes until they were revived from anesthesia and housed in separate cages by the group.

Cell culture and reagents

The mouse microglial cell-line BV2 were cultivated in Dulbecco's Modified Eagle's Medium (DMEM) (#C11995500BT, Gibco) containing 10% fetal bovine serum (FBS) (#04-001-IACS, Biological Industries) and 1% penicillin-streptomycin and maintained under the stable environment with 37°C and 5% CO2. Cell stimulation was induced 10μM oxy-Hb (#JP0200, Jinpin Chemical Technology Co., Ltd. CN). zVAD-FMK was selected (# C1202 Beyotime CN) 30umol/ml, Necrostatin-1 (#SC4359 Beyotime CN) 30μM/ml, the above reagents were added to microglia cultured inappropriate well plates for modeling.

Western blot

The harvested cells or animal tissues were lysed on ice with RIPA lysis solution for 30 min and then centrifuged at 12000g for 10 min at 4°C. The protein supernatant was added to the loading buffer and denatured at 100°C for 5 min. The samples were added to SDS-PAGE gel for electrophoresis, after which the proteins were transferred to PVDF membrane, 5% skim milk powder was blocked for 1 h, and then overnight at 4°C with the following primary antibody: rabbit polyclonal anti-RIPK1 (1:1000 #17519-1-AP Proteintech CN), rabbit polyclonal anti-RIPK3 (1:1000 #17563-1-AP Proteintech CN), Bak1 Rabbit mAb (1:1000 #12105 CST USA), Phospho-MLKL(Ser345) Rabbit mAb (1:1000 #37333 CST USA), Rabbit Polyclonal anti-Thrombospondin 1 (1:1000 # 18304-1-AP Proteintech CN), Rabbit Polyclonal anti-Beta Tubulin (1:5000 # 10094-1-AP Proteintech CN). The appropriate secondary antibody (1:5000) was selected and incubated for 1h, X-ray film and Image J software (NIH) were used for detecting and quantifying, respectively.

Propidium iodide staining

Intraperitoneal injection of pyridinium iodide (PI 10mg/kg) 1h before sacrificing mice after SAH 24h, Brain tissue was obtained after cardiac perfusion with ice PBS and immediately embedded by OCT, avoiding light in sections, Brain sections were cut at 10μm intervals near the optic chiasma. The sections were fixed with 4% paraformaldehyde for 10 min, washed with PBS 3 times×10 min, 0.3% TritonX-100 for 10 min, and then blocked with 10% goat serum for 1h, Anti-IBA1 (1:500 #ab178846 Abcam USA) overnight at 4°C, fluorescent secondary antibody Goat anti-Rabbit (H+L 488) (1:200 #ab150077 Abcam USA) incubated for 1h at room temperature, DAPI blocked, fluorescence microscopy photographed(Olympus, Japan) and propidium iodide-positive microglia were quantified in puncture bleeding injury region from 200× in three brain sections per mice.

Oxyhemoglobin stimulated BV2 cells for 24h. 1× PI staining working solution (#C1056 Beyotime) and Hoechst 33342 (#C1027 Beyotime) were added, incubated for 20min at 37°C, avoiding light, and PI-positive BV2 cells were photographed by fluorescence microscopy.

Immunofluorescence staining

Mice 24h after SAH, ice PBS and 4% paraformaldehyde heart perfusion and immersed mouse brain for 2h, 30% sucrose dehydration overnight at 4°C, OCT embedding, brain tissue section 10μm, 0.01M Sodium citrate antigen repair, 0.3% TritonX-100 10min then 10% goat serum blocked for 1h. Anti-IBA1 (1:500 #ab178846 Abcam USA), anti-MLKL (1:100 #66675-1-Ig proteintech CN) overnight at 4°C, fluorescent secondary antibody Goat anti-Rabbit (H+L) (1:200 #ab150077 Abcam USA) and Goat anti- Mouse (H+L) (1:200 #ab150116 Abcam USA) incubated for 1h at room temperature, DAPI blocked, The MLKL co-localizes with IBA1 in microglia was observed using a fluorescent microscope (Olympus Japan).

Reactive oxygen measurement

BV2 cells after 24h of oxyhemoglobin stimulation, Removal of supernatant, add the working assay solution to the cells according to the Reactive Oxygen Species Assay Kit (#S0033S Beyotime CN) manufacturer's instruction. Incubate for 20min at 37℃, avoiding light, Wash cells three times with serum-free medium after incubation; Fluorescence situation was examined using a fluorescent microscope (Olympus, Japan).

Bak1-KO cell line construction

Bak1 sgRNA was designed using the online tool (http://crispr-era.stanford.edu/), and the target sequence 5'-TCGGGGTCTTCGTCTTTGCA-3' was cloned into the plasmid lentiGuide-Puro (addgene #52963 USA). The plasmid vector was then transfected with liposomal transfection reagent LipoFiter3.0 (HANBIO, CN) in 293T cells, and supernatants containing viral particles were collected every 24 h for three days after transfection. Infection of BV2 cells after concentrating and purifying the virus. The Cas9 protein expression plasmid lentiCas9-Blast was constructed and infected with BV2 cells, in the same way, followed by puromycin or blasticidin selection. Sequencing to identify completed mutant BV2 cell lines, WB to detect Bak1 protein knockout efficiency.

Bak1 and THBS1 knockdown

THBS1 and Bak1 shRNA were designed using the online tool (https://www.sigmaaldrich.cn/cn/zh). THBS1 target sequence 5'-GCCAGAACTCGGTTACCATCT-3', Bak1 target sequence 5'-GCTCTCATCGGAGATGATATT-3', and the scrambled control sequence 5'-TTCTCCGAACGTGTCACGT-3' were cloned into the lentiviral shRNA expression vector plko.1. the plasmid vector was then transfected with liposomal transfection reagent lipofiter3 (HANBIO, CN) in 293T cells, collecting virus supernatant every 24h. after virus concentration and purification, THBS1 virus-infected Bak1-ko cell line, NC negative control, and Bak1-KD virus-infected BV2 cells, RT-qPCR and WB detected knockdown efficiency.

RT-qPCR

HiScript III-RT SuperMix synthesized cDNA for qPCR (+gDNA wiper) (#R323, Vazyme Biotech Co., Ltd); reactions were performed on LightCycle®96 (Roche) using ChamQ Universal SYBR qPCR Master Mix

(#Q711, Vazyme Biotech Co., Ltd). The result was analyzed using the $2^{-\Delta\Delta Cq}$, gene expression was normalized to β-actin and presented as a fold change relative to control.

Co-immunoprecipitation

Stimulation of BV2 cells with oxyhemoglobin for 24h, Whole-cell lysates were extracted with IP lysis buffer (NP-40 1%, Tris-HCL 8.0 50mmol/ml, Glycerin 10%, NaCl 150mmol/ml, EDTA 5mmol/ml) supplemented with Protease and phosphatase inhibitors (#P1045, Beyotime). The lysates were sonicated and centrifuged at 12000×g for 10min at 4 °C. The BCA Assay Reagent (#P0012S, Beyotime) was used to determine protein concentration. Take 10% of the total volume of lysate as input. 2mg of whole protein was made for the IgG and IP groups, respectively. Add Rabbit control IgG antibody (1:200 #AC005, ABclonal) anti-RIPK3 (anti-RIPK3 1:200 #17563-1-AP Proteintech CN), 4°C overnight. Antibody-protein mixture is incubated in the appropriate volume of Dynabeads Protein A (#10001D, Invitrogen™) for 30 minutes at room temperature. After washing the beads three times, the samples were denatured at 100°C for 5 min using a 5×SDS loading buffer, and WB detected the pull-down proteins.

Cell viability assays

Cells were seeded at a density of 5×10^3 cells/well in 96-well plates. After overnight incubation, fresh medium containing Oxyhemoglobin was added, and the plates were maintained for 0, 12,24h. Add CCK8 reagent (1:100 #HB-CCK-8-10 HANBIO CN) and incubate for 2 hours protected from light, measure the OD450 value, and compare the relative CCK8 values at each time point.

ELISA

TNFα ELISA kit, IL-6 ELISA kit, IL-1β ELISA kit were obtained from NEOBIOSCIENCE CN (#EMC001b.96, #EMC102a.96, # EMC004.96); subsequent testing follows manufacturer's protocols. The same number of BV2 cells were seeded into the culture well plates, and the cell supernatant was collected for detection after 24h of hemoglobin stimulation. The mice's brain tissues were obtained from SAH molds for 24h, lysed by RIPA, and BCA measured protein concentrations. Brain tissue lysates with the same protein content were taken for subsequent assays. The samples were added to the test wells, and the standard wells were set up simultaneously. After the operation, according to the kit's instructions, the OD450 values were measured, and the contents of IL-6, IL-1β, and TNFα were calculated according to the standard curve.

RNA-Seq

Microglia were seeded in a 6-well plate, and after 12h for complete cell wall adhesion, Oxy-Hb stimulated the cells and reached the scheduled stimulation time. Cellular RNA was extracted using RNAeasy Isolation Reagent (#R701-02, Vazyme Biotech Co., Ltd) according to the manufacturer's instructions. The Universal V6 RNA-seq Library Prep Kit for Illumina (#NR604-02, Vazyme Biotech Co., Ltd) was used for library preparation. Briefly, the samples were normalized at a 500 ng/ml concentration. First, samples

were subjected to a tagmentation redaction, indexed, and PCR amplified. Libraries were then purified with VAHTS DNA Clean Beads (#N411-02, Vazyme Biotech Co., Ltd). QC checks for the library preparations included electrophoresis (Agilent Technologies 2100 Bioanalyzer) or library quantification. The Novogene (Beijing CN) sequence was sequenced on an Illumina HiSeq 1500 high-throughput sequencing system.

Transcriptome analysis

The raw fastq files were trimmed using trim galore (version 1.18) to remove adaptor sequences and low-quality reads. Then FastQC (version 0.11.9) was used for quality control. The remaining reads were aligned to the GRCm38 mouse genome using HISAT2 (v2.2.0) with default parameters and filtered with samtools (version 1.10, parameters used: samtools view -F 1804 -f 2 -q 30). Gene counts were calculated from the mapped reads using featureCounts (v2.0.1) with the Ensembl gene annotation (version mm10). Subsequently, TPM (Transcripts Per Kilobase of exon model per Million mapped reads) in each gene was calculated for subsequent analysis. Differential expressed genes (DEGs) was evaluated using DESeq2 package in R (version 4.2.0), using adjusted $P < 0.05$ and $|log2FC| > 1$ as cutoffs to define the DEGs.

GSEA analysis

GSEA uses the expression matrix obtained by cluster profile package in R software to carry out GSEA based on biological processes in gene ontology (GO-BP) and based on the Kyoto Encyclopedia of Gene and Genome (KEGG) signal pathway, respectively, to obtain the enrichment results of differentially expressed genes in GO functional annotation and KEGG pathway obtained by differential analysis between NC group and KD group. The gene sequence was arranged according to the descending order of multiple gene expression changes (foldchange, FC) in the Bak1-KD group compared with the NC group. The statistical method was Fisher exact probability test, and error detection rate (false discovery rate, FDR) was used to correct.

Statistical analysis

GraphPad Prism 8 was used for statistical analysis. We used an unpaired two-tailed t-test to compare two groups, and a one-way ANOVA was applied to compare three or more independent groups. Bar graphs were described as mean ± Standard error of the mean (SEM) of at least three independent experiments. Statistically significant changes relative to a negative control were represented with $P < 0.05$.

Result

Experimental subarachnoid hemorrhage induces necroptosis of microglia

Previous studies have reported that subarachnoid hemorrhage induces neuronal necroptosis and elevates the expression of RIPK1/RIPK3[12]**.** However, the microglia necroptosis after subarachnoid hemorrhage is unclear. We established 24h, 48h, and 72h mouse subarachnoid hemorrhage models during early brain injury. WB detected the expression of necroptosis-related proteins RIPK1/RIPK3, and similar to the reported results, RIPK1 was elevated 24 h after bleeding (Fig.1B), but the expression of RIPK3 was not

significantly upregulated (Fig.1B). PI staining is commonly used to label necrotic cells, and PI-positive cells were found in the area of injury following subarachnoid hemorrhage. Immunofluorescence suggests co-localization of microglia marker IBA1 with PI, indicative of microglial cell necrosis (Fig.1C). MLKL is a functional executive protein of necroptosis, and immunofluorescence revealed that MLKL co-localized with IBA1 after 24 h of subarachnoid hemorrhage (Fig.1D). The Sham group did not observe the phenomenon, suggesting that microglia suffered necroptosis. Neurological function scores decreased in mice after subarachnoid hemorrhage (Fig.1E), suggesting that necroptosis of microglia may be associated with reduced neurological function scores.

In vivo knockdown microglia Bak1 protein attenuates necroptosis and neuroinflammation

It has been documented that Bak1 contributes to amplifying the biological process of necroptosis[13]. We hypothesize that disrupting Bak1 may diminish microglia necrosis and its downstream inflammatory response in subarachnoid hemorrhage. Western blot (WB) found elevated Bak1 in subarachnoid hemorrhage at 24h (Fig.2A), Suggesting that subarachnoid hemorrhage induces increased expression of Bak1. However, whether Bak1 regulates microglial cell necrosis and inflammation is unclear. The adeno-associated virus was used to precisely inhibit Bak1 protein production in mouse microglia; following modeling, there was no statistical difference in the degree of SAH between the NC control and Bak1 knockdown groups (Fig.2B). The number of PI and IBA1 co-localized microglia in the Bak1-KD group mice was lower than in the Sham group ($P<0.05$) (Fig.2C), implying that Bak1 knockdown reduced microglia necrosis. WB revealed that RIPK1 expression was downregulated in Bak1 knockdown mice($P<0.05$) (Fig.2E), and RIPK3 expression was mildly downregulated compared to the Sham group, but there was no significant statistical difference. Microglia activation can mediate an excessive inflammatory response. At the same time, the release of pro-inflammatory factors such as Tumor Necrosis Factor Alpha (TNFα) can initiate necroptosis through the TNFα-TNFR1 ligand-receptor signaling pathway, exacerbating the injury[14]. ELISA revealed that interference with microglia Bak1 protein decreased the expression of pro-inflammatory factors Interleukin-6 (IL-6), Interleukin-1 beta (IL-1β), and TNFα after subarachnoid hemorrhage and increased the neurological function score in mice compared with the NC group (Fig.2D, F).

Oxyhemoglobin stimulation induces necroptosis and oxidative stress in microglia

The role of microglial necroptosis in neuroinflammation following a subarachnoid hemorrhage is currently unknown. To investigate the occurrence of necroptosis, we stimulated BV2 microglia with oxyhemoglobin. PI staining revealed that microglia necrosis increased after 24 hours of stimulation (Fig.3 A); WB results revealed that the expression of the phosphorylated pseudokinase mixed lineage kinase domain-like protein (p-MLKL), the functional execution molecule of necroptosis, was elevated ($P<0.05$), but the expression of RIPK1/RIPK3 was not significantly altered (Fig.3B). We assessed intracellular ATP content because p-MLKL can translocate to mitochondria and trigger mitochondrial damage via mitochondrial MPTP; ATP levels reduced after 24 hours of oxyhemoglobin stimulation compared to the control group ($P<0.05$) (Fig.3C). The CCK8 assay reveals that microglia have lower cell viability after

oxyhemoglobin activation (P<0.05) (Fig.3C). In parallel, oxidative stress is a crucial process downstream of necroptosis[15]. The DCFH-DA probe suggests that cellular reactive oxygen species increase after oxyhemoglobin stimulation and microglia suffer significant oxidative stress (Fig.3D).

Necroptosis mediates pro-inflammatory phenotype transformation of microglia to exacerbate neuroinflammation

Classical inflammatory pathways, such as toll-like receptor signaling pathways (hemoglobin-associated receptors), trigger microglia necroptosis and increase neuroinflammation.[16] So we speculate that microglia necroptosis may promote microglia pro-inflammatory phenotype transformation. At 12h and 24h following oxyhemoglobin stimulation, RT-qPCR detected the expression of pro-inflammatory phenotype genes (*Irg1*, *Gpr84*) and anti-inflammatory phenotype genes (*Arg1*, *Mrc1*) in BV2, and pro-inflammatory genes (*Irg1*, *Gpr84*) were found to be elevated (P<0.05) (Fig.4A). Anti-inflammatory genes (*Arg1*, *Mrc1*) were downregulated following stimulation (P<0.05) (Fig.4A), while pro-inflammatory factor transcripts *IL-6*, *IL-1β*, and *TNFa* were upregulated (P<0.05) (Fig.4B). We utilized zVAD-FMK, a commonly used necroptosis inducer, to stimulate microglia together with oxyhemoglobin and discovered that it increased *IL-6*, *IL-1β*, and *TNFa* in microglia(P<0.05) (Fig.4C). The pro-inflammatory phenotype of microglia can trigger the release of numerous chemokines and promote peripheral immune cell infiltration. RT-qPCR analysis showed that oxyhemoglobin stimulation increases the expression of chemokines *Ccl2*, *Ccl5*, *Cxcl2*, and chemokine receptors *Ccr5* (P<0.05) (Fig.4D).

In vitro knockout of Bak1 alleviates microglia necroptosis and oxidative stress

Bak1 is a critical molecule in regulating mitochondrial MPTP in the BCL-2 family proteins associated with necroptosis mitochondrial damage[17]. WB data showed that Bak1 expression elevated 24 hours after oxyhemoglobin stimulation in microglia, and that Bak1 expression increased further after zVAD-FMK induction (Fig.5A). As Bak1 and MLKL can localize to mitochondria and mediate mitochondrial damage[10], it is unclear whether Bak1 interacts with RIPK3. We performed co-immunoprecipitation tests on RIPK3 protein and found that RIPK3 can pull down RIPK1 and Bak1 with oxyhemoglobin stimulation. (Fig.5B). The results suggest that Bak1 may be involved in the biological processes associated with necroptosis. We constructed a Bak1-KO microglia cell line, and PI assay revealed that deletion of Bak1 reduced the number of oxyhemoglobin-induced PI-positive cells in microglia (Fig.5C). CCK8 assay reveals that Bak1 deletion increases cell survival that declines following oxyhemoglobin stimulation, while ATP assay implies that Bak1 deletion enhances mitochondrial function in microglia (Fig.5D). Also, as a downstream damaging mechanism of necroptosis, reactive oxygen was significantly downregulated in Bak1 deleted microglia (Fig.5E). The p-MLKL content was measured utilizing WB, and p-MLKL was found to be down-regulated in the Bak1-KO cell group, whereas RIPK1, RIPK3 were not significantly altered (P<0.05) (Fig.5F). These data suggest that deletion of Bak1 alleviates necroptosis and oxidative stress in BV2 cells.

Knockout of BV2 microglia Bak1 attenuates pro-inflammatory phenotype transformation and neuroinflammation

Microglia necroptosis is associated with pro-inflammatory phenotype transformation and neuroinflammation. The RT-qPCR analysis demonstrates that Bak1-KO significantly decreases the expression of zVAD-FMK+ oxyhemoglobin-stimulated proinflammatory phenotype genes (*Gpr84*, *Irg1*) in comparison to WT BV2 ($P<0.05$) (Fig.6A). Chemokines (*Ccl5*, *Ccl2*, *Cxcl2*), chemokine receptor (*Ccr5*), *Nos2* mRNAs were also significantly decreased in Bak1-KO cells($P<0.05$) (Fig.6B). In parallel, ELISA demonstrated that the levels of cellular supernatant pro-inflammatory factors (IL-6, IL-1β, TNFα) were downregulated after Bak1-KO (Fig.6C). Interestingly, when we evaluated the transcription of pro-inflammatory factors in Bak1-KO cells in the presence of zVAD-FMK, we found no difference in the production of *IL-1β* and *TNFα* compared to the DMSO group. In contrast, *IL-6* expression was altered in the same way that it was in WT BV2 cells ($P<0.05$) (Fig.6D), indicating that the deletion of Bak1 seems to downregulate the pro-inflammatory process of necroptosis through blocking the transcription of *IL-1β* and *TNFα*. Overall, the knockout of microglia Bak1 attenuated the pro-inflammatory phenotype and neuroinflammation.

Disruption of Bak1 elevates THBS1 to reduce cellular injury and neuroinflammation

Microglial necroptosis and neuroinflammation are reduced when Bak1 is deleted, but the mechanism is unknown. To identify the biological processes that may be altered as a natural consequence of Bak1 interference, total RNA was analyzed using RNA-Seq following Bak1 knockdown scenarios. We found 118 differentially expressed genes after 12 hours of oxyhemoglobin stimulation, with 52 up-regulated genes and 66 down-regulated genes, and 102 differentially expressed genes at 24 hours, with 36 up-regulated genes and 66 down-regulated genes. The heatmap represents the dynamic differences in gene expression between the NC and Bak1-KD groups at the 12h and 24h time points following oxyhemoglobin stimulation. The hierarchically clustered heatmap detects significant differences in gene expression between the NC and KD groups (whether in 12H or 24H). (Fig.7A). Biological processes (BP) in GO altered by GESA at 12h and 24h under oxyhemoglobin stimulation were examined. Interference with Bak1 resulted in the downregulation of biological processes such as regulation of small GTPase mediated signal transduction, toll-like receptor signaling pathway, cellular response to reactive oxygen species, an innate immune response associated with inflammatory response, and capable of mediating necroptosis at 12h. While biological processes that weaken the inflammatory response and necroptosis were increased, such as negative regulation of the ERK1 and ERK2 cascades, negative regulation of protein kinase B signaling, and negative regulation of the MAPK cascade. Regulation of mitochondrial membrane potential and negative regulation of the intrinsic apoptotic signaling pathway were increased (Fig.7B). We revealed that positive regulation of chemokine production, MAP regulation of MAP kinase activity, receptor signaling pathway via JAK-STAT, receptor signaling pathway via STAT, cellular response to oxidative stress, cellular response to chemical stress, cytokine-mediated signaling pathway, response to cytokine, cellular response to cytokine stimulus, and cellular response to cytokine stimulus were all present in the 24h group. These above-mentioned biological processes associated with the inflammatory response are significantly downregulated (Fig.7B). Based on the GSEA results of up-down differential genes at 12h, a network of biological processes and genes in the top 30 GO was created. We discovered that multiple biological processes linked to necroptosis and tumor necrosis factor in the

network were all connected to the gene THBS1, so we speculated that THBS1 played an essential role after Bak1-KD (Fig.7C). THBS1 regulates endoplasmic reticulum stress as an intracellular protein[18], whereas exocytosis to the extracellular matrix regulates macrophage migration, infiltration, and inflammation[19-21]. In an oxyhemoglobin-stimulated model, WB demonstrates increased THBS1 expression after Bak1-KO. THBS1 expression was downregulated after zVAD+oxyhemoglobin induction, whereas the necroptosis inhibitor Nec-1 increased THBS1, indicating that necroptosis downregulates THBS1 ($P<0.05$) (Fig.7D). We knocked down THBS1 in the Bak1-KO cell line; CCK8 results suggest that THBS1 knockdown reduced cell viability while intracellular ATP content was downregulated compared to the Bak1-KO cell line (Fig.7E). The alteration of pro-inflammatory factors by RT-qPCR demonstrated that with the knockdown of THBS1, the expression of *IL-6*, *IL-1β*, and *TNFα* down-regulated by knockout Bak1 partially increased (Fig.7F). These results suggest that deletion of Bak1 can attenuate necroptosis-induced cell injury by elevating THBS1, while THBS1 is involved in the pathophysiological process of necroptosis.

Discussion

In the present study, we explored some of the mechanisms by which Bak1 protein regulates microglial necroptosis and neuroinflammation after SAH in vivo and in vitro.) The co-localization of PI and MLKL with microglia IBA1 during SAH demonstrates that microglia undergo necroptosis and subsequently impair neurological function.) Stimulation of microglia with oxyhemoglobin promotes necroptosis, increases oxidative stress, transforms microglia into a pro-inflammatory phenotype, and exacerbates neuroinflammation.) Necroptosis increases Bak1 expression and the interaction between Bak1 and RIPK3. Microglial Bak1 protein deficiency decreased p-MLKL content, reduced ROS, decreased expression of pro-inflammatory phenotype genes *Irg1* and *Gpr84*, attenuated neuroinflammation, and improved neurological scores after SAH.) RNA-Seq analysis indicates that the Bak1 protein regulates various inflammatory pathways. Additionally, we demonstrate that necroptosis decreases the expression of candidate gene *Thbs1*, interfering with candidate gene *Thbs1* cancels off the positive effects of Bak1 deletion. Our data suggest that silencing the Bak1 protein, which is mediated in part by increased THBS1, can reduce necroptosis and neuroinflammation in microglia following SAH.

Inflammation may play a significant role in both the acute and chronic phases of neural injury associated with SAH, according to emerging evidence[22]. As the earliest events in pathophysiology, molecules from extravasated blood and damaged brain appear to be the primary initiators of the inflammatory cascade, accompanied by the activation and infiltration of immune cells at the site of injury[23]; this vicious cycle of inflammation almost certainly contributes to nearly every mechanism of SAH, including apoptotic or necroptosis[24, 25]. Necroptosis, is a pro-inflammatory programmed death with morphology similar to cellular necrosis and can be induced by exogenous ligands and intracellular stress, resulting in caspase-independent cell death[26]. Following subarachnoid hemorrhage, necroptosis accelerates early brain injury, exacerbates disruption of the blood-brain barrier, increases brain edema, exacerbates neuroinflammation, and damages synapses, resulting in neurological deficits[25, 27–29]. However, these investigations did not focus on the role of microglia necroptosis in the modulation of neuroinflammation

following subarachnoid hemorrhage. The current study suggests necroptosis of microglia plays a vital role in neurodegenerative diseases, ischemic stroke, retinopathy, and related neuroinflammation[14, 16, 30]. A single-cell sequencing identified specific subtypes of microglia with high expression of the necroptosis-associated genes RIPK3 and MLKL, named sMG2[31]. Based on this evidence, we hypothesize that microglial necroptosis may play a regulatory role in subarachnoid hemorrhage.

Our immune staining reveals that microglia undergo necroptosis following SAH. Activation of microglia and necroptosis might deteriorate the prognosis of neuroinflammatory diseases and exacerbate demyelination[32–34], and microglia-driven cerebral spreading inflammation is a key contributor to secondary brain injury after SAH [35]. Consistent with our finding in vivo, oxyhemoglobin stimulated BV2 microglia increased p-MLKL and the number of PI-positive microglia. Thus, blood components may operate as a predisposing factor for microglial necroptosis. Previous study has reported that released chemokines from microglia can induce infiltration of peripheral immune cells into the damaged area. The chemokines released from microglia after pro-inflammatory transformation can induce infiltration of peripheral immune cells into the damaged area[36]. Additionally, necroptosis often accompanies definite oxidative stress, further aggravating early brain injury after SAH[37, 38]. In our results, the necroptosis inducer zVAD-Fmk coupled with oxyhemoglobin enhanced the reactive oxygen species concentration, pro-inflammatory factors *IL-6*, *IL-1β*, and *TNFα*, in comparison to WT BV2 cells treated with oxyhemoglobin. These findings strongly suggest necroptosis of microglia following SAH promotes microglia pro-inflammatory phenotype transformation, aggravating early neuroinflammation and oxidative stress, which is similar to chronic inflammatory neurological diseases[39].

Recently, a novel concept of necroptosis has been proposed, meaning a combination of apoptosis and necrosis[10]. Bak1, a crucial molecule in regulating apoptosis by releasing a range of mitochondrial contents, is found in the outer mitochondrial membrane. However, mitochondrial DNA (mtDNA) release can mediate downstream inflammatory responses via the cGAS/STING-dependent pathway, separating it from apoptotic immunosilencing[40, 41]. Another study found that silencing Bak1 decreased BV6/Dexa-mediated necroptosis in a time-dependent manner[13]. Our findings indicate that Bak1 plays a role in microglial necroptosis in a hemorrhagic environment and appears to be involved in the development of complex IIb, when RIPK3 protein immunoprecipitation can pull down Bak1. Interestingly, Knockout of Bak1 in BV2 microglia down-regulated necroptosis-induced MLKL phosphorylation, while the expression of RIPK1 and RIPK3 was unchanged, further suggesting that Bak1 is present in contexts in necroptosis vesicle complex b. Furthermore, although necroptosis disrupts cellular integrity, DAMPs-containing cellular contents are released into the surrounding tissue environment, which can activate inflammatory cascade responses [42]. Our results indicate that Bak1 regulates neuroinflammation not only by the inhibition of necroptosis DAMPs, but also by specific intracellular signals that modulate the expression of *IL-1β* and *TNFα*. However, the exact regulatory mechanism was not clear.

RNA-Seq data provided us with new insights. We found that a broad range of pro-inflammatory biological processes, oxidative stress, and biological processes related to mitochondrial membrane potential were altered after Bak1 depletion, consistent with the results obtained in vitro. While some of the biological

processes related to ligand-receptor signaling and regulation of cellular junctions are also altered, we speculate that disturbance of Bak1 can affect the expression of some downstream exocytotic proteins. THBS1, a glycoprotein that regulates macrophage migration and extracellular matrix alterations, was increased after the Bak1 knockout. Recently, THBS1 was reported as a key regulator of the microglial inflammatory response[19, 21]. Our data further suggested that the necroptosis inducer zVAD-FMK downregulated THBS1 expression. Interestingly, after knocking down THBS1, the expression of pro-inflammatory factors was partially reversed. This appears to explain the altered biological processes and receptor-related signals observed in GSEA analysis, suggesting that THBS1 is a downstream molecule of Bak1 regulation of necroptosis-mediated neuroinflammation. Although we discovered that the THBS1-related receptors *CD47*, *CD36*, and *Tgfb1* transcriptional changes in the depletion of Bak1 (data not shown), the particular target of THBS1 in controlling necroptosis remains unknown, and more in-depth regulatory mechanisms need to be further investigated.

Conclusion

Collectively, deletion of microglial Bak1 reduces oxyhemoglobin-induced necroptosis and proinflammatory phenotype transformation, as well as ameliorates necroptosis and neuroinflammation in mice with experimental SAH. We also demonstrated that THBS1 could be a potential downstream molecule of Bak1-related microglial necroptosis. Bak1 is expected to be a potential molecular target for SAH treatment.

Abbreviations

SAH
subarachnoid hemorrhage
Bak1
BCL-2 homologous antagonist-killer protein
RNA-Seq
RNA-sequencing
MLKL
Pseudokinase mixed lineage kinase domain-like protein
p-MLKL
Phosphorylated pseudokinase mixed lineage kinase domain-like protein
THBS1
Thrombospondin 1
RIPK1
Receptor-interacting serine/threonine-protein kinase 1
RIPK3
Receptor-interacting serine/threonine-protein kinase 3
DAMPs

Damage-associated molecular patterns

MOMP

Mitochondrial outer membrane permeability

MPTP

Mitochondrial Permeability Transition Pore

AAV

Adeno-associated virus

GSEA

Gene Set Enrichment Analysis

NLRP3

NACHT, LRR and PYD domains-containing protein 3

KD

Knockdown

KO

Knockout

Oxy-Hb

Oxyhemoglobin

DEGs heatmap

Differentially expressed genes heatmap

Declarations

Acknowledgments

We would like to thank all the members of the Laboratory of Neurological Diseases and Brain Function, The Affiliated Hospital of Southwest Medical University, Luzhou, China.

Ethics approval and consent to participate

All experimental animal procedures involved in this study are approved by the China Committee for the Care and Use of Laboratory Animals and follow the regulatory requirements of the Animal Committee of the Ethics Committee of Southwest Medical University (permit number: SYXK (Chuan) 2018–065).

Consent for publication

Not applicable.

Availability of data and materials

The datasets used and/or analyzed during the current study are available from the corresponding author on reasonable request.

Competing interests

No potential conflict of interest was reported by the authors.

Funding

This work was supported by grants from the Young Elite Scientist Sponsorship Program by the China Association for Science and Technology (YESS20200178) and the National Natural Science Foundation of China (81971132); the Sichuan Science and Technology Program (2021ZYD0106); Luzhou Government-Southwest Medical University Strategic Cooperation Project and of Southwest Medical University Project (2021LZXNYD-P01, 2021ZKZD013); Luzhou Science and Technology Program (2020-RCM-68).

Authors' contributions

QXC designed the study and prepared the manuscript. QXC, TQK, ZLH performed the experiments. QXC, ZLH completed bioinformatics analysis, QXC, TQK contributed equally to this work. KCH, XYK, ZLF were involved in experiment performance and data collection. YSG, PJH, JY were responsible for the supervision of the entire project and were involved in the study design, data interpretation, manuscript preparation, and funding. All authors read and approved the final manuscript.

References

1. Pang J, Peng J, Yang P, Kuai L, Chen L, Zhang JH, Jiang Y: **White Matter Injury in Early Brain Injury after Subarachnoid Hemorrhage.** *Cell Transplant* 2019, **28:**26-35.
2. Macdonald RL, Schweizer TA: **Spontaneous subarachnoid haemorrhage.** *Lancet* 2017, **389:**655-666.
3. Li Y, Liu Y, Wu P, Tian Y, Liu B, Wang J, Bihl J, Shi H: **Inhibition of Ferroptosis Alleviates Early Brain Injury After Subarachnoid Hemorrhage In Vitro and In Vivo via Reduction of Lipid Peroxidation.** *Cell Mol Neurobiol* 2021, **41:**263-278.
4. Xu P, Hong Y, Xie Y, Yuan K, Li J, Sun R, Zhang X, Shi X, Li R, Wu J, et al: **TREM-1 Exacerbates Neuroinflammatory Injury via NLRP3 Inflammasome-Mediated Pyroptosis in Experimental Subarachnoid Hemorrhage.** *Transl Stroke Res* 2021, **12:**643-659.
5. Chen T, Pan H, Li J, Xu H, Jin H, Qian C, Yan F, Chen J, Wang C, Chen J, et al: **Inhibiting of RIPK3 attenuates early brain injury following subarachnoid hemorrhage: Possibly through alleviating necroptosis.** *Biomed Pharmacother* 2018, **107:**563-570.
6. Yuan J, Amin P, Ofengeim D: **Necroptosis and RIPK1-mediated neuroinflammation in CNS diseases.** *Nat Rev Neurosci* 2019, **20:**19-33.
7. Galluzzi L, Vitale I, Aaronson SA, Abrams JM, Adam D, Agostinis P, Alnemri ES, Altucci L, Amelio I, Andrews DW, et al: **Molecular mechanisms of cell death: recommendations of the Nomenclature Committee on Cell Death 2018.** *Cell Death Differ* 2018, **25:**486-541.
8. Dionisio PA, Amaral JD, Rodrigues CMP: **Molecular mechanisms of necroptosis and relevance for neurodegenerative diseases.** *Int Rev Cell Mol Biol* 2020, **353:**31-82.

9. Vince JE, De Nardo D, Gao W, Vince AJ, Hall C, McArthur K, Simpson D, Vijayaraj S, Lindqvist LM, Bouillet P, et al: **The Mitochondrial Apoptotic Effectors BAX/BAK Activate Caspase-3 and -7 to Trigger NLRP3 Inflammasome and Caspase-8 Driven IL-1beta Activation.** *Cell Rep* 2018, **25:**2339-2353 e2334.
10. Karch J, Kanisicak O, Brody MJ, Sargent MA, Michael DM, Molkentin JD: **Necroptosis Interfaces with MOMP and the MPTP in Mediating Cell Death.** *PLoS One* 2015, **10:**e0130520.
11. Peng J, Wu Y, Pang J, Sun X, Chen L, Chen Y, Tang J, Zhang JH, Jiang Y: **Single clip: An improvement of the filament-perforation mouse subarachnoid haemorrhage model.** *Brain Inj* 2019, **33:**701-711.
12. Chen F, Su X, Lin Z, Lin Y, Yu L, Cai J, Kang D, Hu L: **Necrostatin-1 attenuates early brain injury after subarachnoid hemorrhage in rats by inhibiting necroptosis.** *Neuropsychiatr Dis Treat* 2017, **13:**1771-1782.
13. Rohde K, Kleinesudeik L, Roesler S, Lowe O, Heidler J, Schroder K, Wittig I, Drose S, Fulda S: **A Bak-dependent mitochondrial amplification step contributes to Smac mimetic/glucocorticoid-induced necroptosis.** *Cell Death Differ* 2017, **24:**83-97.
14. Chen AQ, Fang Z, Chen XL, Yang S, Zhou YF, Mao L, Xia YP, Jin HJ, Li YN, You MF, et al: **Microglia-derived TNF-alpha mediates endothelial necroptosis aggravating blood brain-barrier disruption after ischemic stroke.** *Cell Death Dis* 2019, **10:**487.
15. Zhang T, Zhang Y, Cui M, Jin L, Wang Y, Lv F, Liu Y, Zheng W, Shang H, Zhang J, et al: **CaMKII is a RIP3 substrate mediating ischemia- and oxidative stress-induced myocardial necroptosis.** *Nat Med* 2016, **22:**175-182.
16. Huang Z, Zhou T, Sun X, Zheng Y, Cheng B, Li M, Liu X, He C: **Necroptosis in microglia contributes to neuroinflammation and retinal degeneration through TLR4 activation.** *Cell Death Differ* 2018, **25:**180-189.
17. Tischner D, Manzl C, Soratroi C, Villunger A, Krumschnabel G: **Necrosis-like death can engage multiple pro-apoptotic Bcl-2 protein family members.** *Apoptosis* 2012, **17:**1197-1209.
18. Lynch JM, Maillet M, Vanhoutte D, Schloemer A, Sargent MA, Blair NS, Lynch KA, Okada T, Aronow BJ, Osinska H, et al: **A thrombospondin-dependent pathway for a protective ER stress response.** *Cell* 2012, **149:**1257-1268.
19. Xiao M, Zhang J, Chen W, Chen W: **M1-like tumor-associated macrophages activated by exosome-transferred THBS1 promote malignant migration in oral squamous cell carcinoma.** *J Exp Clin Cancer Res* 2018, **37:**143.
20. You Y, Tian Z, Du Z, Wu K, Xu G, Dai M, Wang Y, Xiao M: **M1-like tumor-associated macrophages cascade a mesenchymal/stem-like phenotype of oral squamous cell carcinoma via the IL6/Stat3/THBS1 feedback loop.** *J Exp Clin Cancer Res* 2022, **41:**10.
21. Ju Y, Tang Z, Dai X, Gao H, Zhang J, Liu Y, Yang Y, Ni N, Zhang D, Wang Y, et al: **Protection against light-induced retinal degeneration via dual anti-inflammatory and anti-angiogenic functions of thrombospondin-1.** *Br J Pharmacol* 2020.

22. Chaudhry SR, Lehecka M, Niemela M, Muhammad S: **Sterile Inflammation, Potential Target in Aneurysmal Subarachnoid Hemorrhage.** *World Neurosurg* 2019, **123:**159-160.
23. Schneider UC, Xu R, Vajkoczy P: **Inflammatory Events Following Subarachnoid Hemorrhage (SAH).** *Curr Neuropharmacol* 2018, **16:**1385-1395.
24. Liu L, Zhang P, Zhang Z, Liang Y, Chen H, He Z, Sun X, Guo Z, Deng Y: **5-Lipoxygenase inhibition reduces inflammation and neuronal apoptosis via AKT signaling after subarachnoid hemorrhage in rats.** *Aging (Albany NY)* 2021, **13:**11752-11761.
25. Yuan S, Yu Z, Zhang Z, Zhang J, Zhang P, Li X, Li H, Shen H, Chen G: **RIP3 participates in early brain injury after experimental subarachnoid hemorrhage in rats by inducing necroptosis.** *Neurobiol Dis* 2019, **129:**144-158.
26. Liu C, Zhang K, Shen H, Yao X, Sun Q, Chen G: **Necroptosis: A novel manner of cell death, associated with stroke (Review).** *Int J Mol Med* 2018, **41:**624-630.
27. Xu H, Cai Y, Yu M, Sun J, Cai J, Li J, Qin B, Ying G, Chen T, Shen Y, et al: **Celastrol protects against early brain injury after subarachnoid hemorrhage in rats through alleviating blood-brain barrier disruption and blocking necroptosis.** *Aging (Albany NY)* 2021, **13:**16816-16833.
28. Chen J, Jin H, Xu H, Peng Y, Jie L, Xu D, Chen L, Li T, Fan L, He P, et al: **The Neuroprotective Effects of Necrostatin-1 on Subarachnoid Hemorrhage in Rats Are Possibly Mediated by Preventing Blood-Brain Barrier Disruption and RIP3-Mediated Necroptosis.** *Cell Transplant* 2019, **28:**1358-1372.
29. Yang C, Li T, Xue H, Wang L, Deng L, Xie Y, Bai X, Xin D, Yuan H, Qiu J, et al: **Inhibition of Necroptosis Rescues SAH-Induced Synaptic Impairments in Hippocampus via CREB-BDNF Pathway.** *Front Neurosci* 2018, **12:**990.
30. Lloyd AF, Davies CL, Holloway RK, Labrak Y, Ireland G, Carradori D, Dillenburg A, Borger E, Soong D, Richardson JC, et al: **Central nervous system regeneration is driven by microglia necroptosis and repopulation.** *Nat Neurosci* 2019, **22:**1046-1052.
31. He C, Liu Y, Huang Z, Yang Z, Zhou T, Liu S, Hao Z, Wang J, Feng Q, Liu Y, et al: **A specific RIP3(+) subpopulation of microglia promotes retinopathy through a hypoxia-triggered necroptotic mechanism.** *Proc Natl Acad Sci U S A* 2021, **118**.
32. Frakes AE, Ferraiuolo L, Haidet-Phillips AM, Schmelzer L, Braun L, Miranda CJ, Ladner KJ, Bevan AK, Foust KD, Godbout JP, et al: **Microglia induce motor neuron death via the classical NF-kappaB pathway in amyotrophic lateral sclerosis.** *Neuron* 2014, **81:**1009-1023.
33. Miron VE, Boyd A, Zhao JW, Yuen TJ, Ruckh JM, Shadrach JL, van Wijngaarden P, Wagers AJ, Williams A, Franklin RJM, Ffrench-Constant C: **M2 microglia and macrophages drive oligodendrocyte differentiation during CNS remyelination.** *Nat Neurosci* 2013, **16:**1211-1218.
34. Dhib-Jalbut S, Kalvakolanu DV: **Microglia and necroptosis: The culprits of neuronal cell death in multiple sclerosis.** *Cytokine* 2015, **76:**583-584.
35. Heinz R, Brandenburg S, Nieminen-Kelha M, Kremenetskaia I, Boehm-Sturm P, Vajkoczy P, Schneider UC: **Microglia as target for anti-inflammatory approaches to prevent secondary brain injury after subarachnoid hemorrhage (SAH).** *J Neuroinflammation* 2021, **18:**36.

36. Shields DC, Haque A, Banik NL: **Neuroinflammatory responses of microglia in central nervous system trauma.** *J Cereb Blood Flow Metab* 2020, **40:**S25-S33.

37. Li X, Cheng S, Hu H, Zhang X, Xu J, Wang R, Zhang P: **Progranulin protects against cerebral ischemia-reperfusion (I/R) injury by inhibiting necroptosis and oxidative stress.** *Biochem Biophys Res Commun* 2020, **521:**569-576.

38. Shindo R, Kakehashi H, Okumura K, Kumagai Y, Nakano H: **Critical contribution of oxidative stress to TNFalpha-induced necroptosis downstream of RIPK1 activation.** *Biochem Biophys Res Commun* 2013, **436:**212-216.

39. Mifflin L, Hu Z, Dufort C, Hession CC, Walker AJ, Niu K, Zhu H, Liu N, Liu JS, Levin JZ, et al: **A RIPK1-regulated inflammatory microglial state in amyotrophic lateral sclerosis.** *Proc Natl Acad Sci U S A* 2021, **118**.

40. Green DR, Kroemer G: **The pathophysiology of mitochondrial cell death.** *Science* 2004, **305:**626-629.

41. White MJ, McArthur K, Metcalf D, Lane RM, Cambier JC, Herold MJ, van Delft MF, Bedoui S, Lessene G, Ritchie ME, et al: **Apoptotic caspases suppress mtDNA-induced STING-mediated type I IFN production.** *Cell* 2014, **159:**1549-1562.

42. Pasparakis M, Vandenabeele P: **Necroptosis and its role in inflammation.** *Nature* 2015, **517:**311-320.

Figures

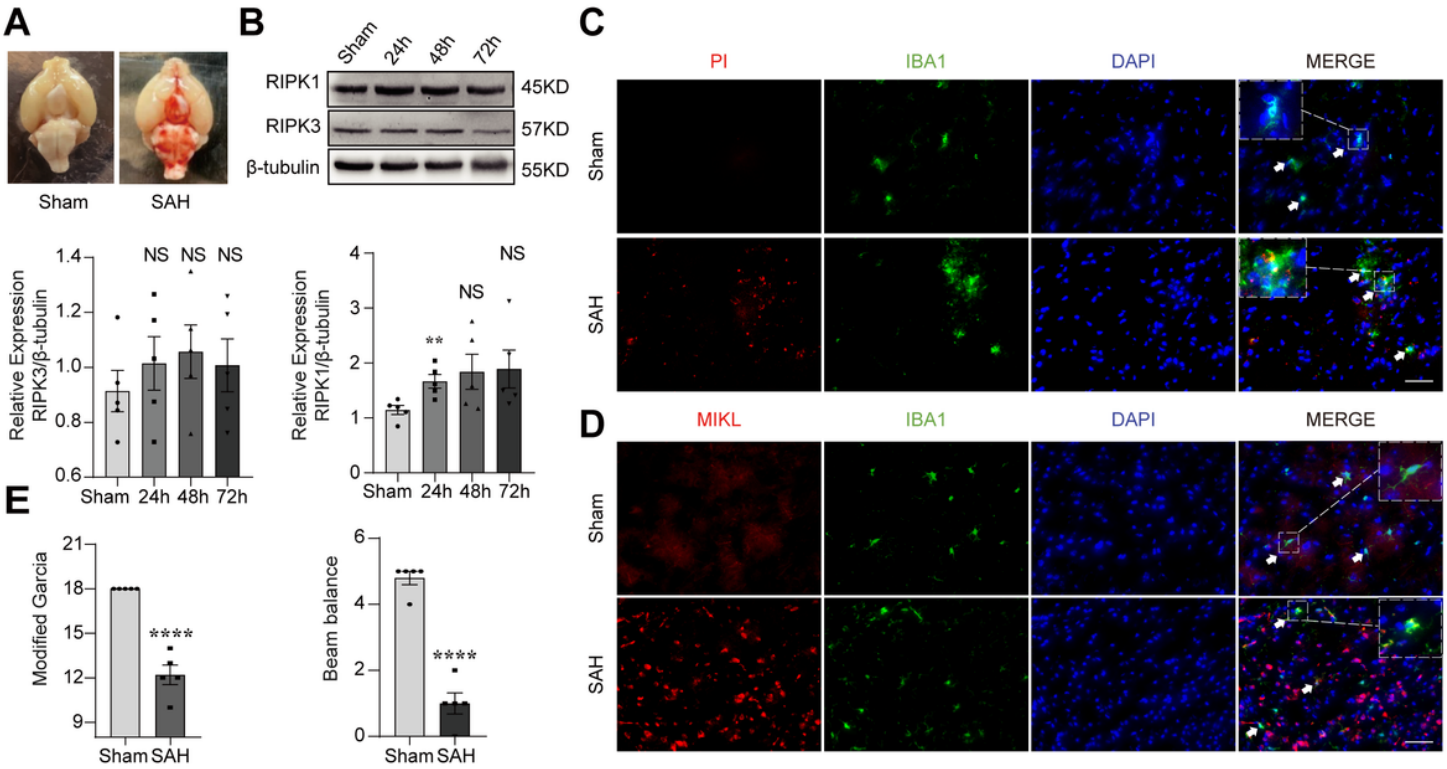

Figure 1

Subarachnoid hemorrhage induces microglial necroptosis. A Sham surgery with mice, no blood clots were found, but mice administered SAH had a massive blood clot in the circle of Willis and on the ventral brainstem surface. The left hemisphere was used for subsequent experiments. **B** Time course of RIPK1, RIPK3 expression in the brain following SAH. The vertical ordinates represent the relative densities of these proteins. n=5 for each group. **P<0.01 versus the Sham group. NS=no significant. **C** Immunofluorescence staining of PI and IBA1 co-localization. Scale bar=50μm. Magnification×200. n=3 in each group. **D** Immunofluorescence staining of MLKL and IBA1 co-localization. Scale bar=50μm. Magnification ×200. n=3 in each group. **E** Neurological function score after 24 hours of SAH. n=5 for each group. ****P<0.0001 versus the Sham group.

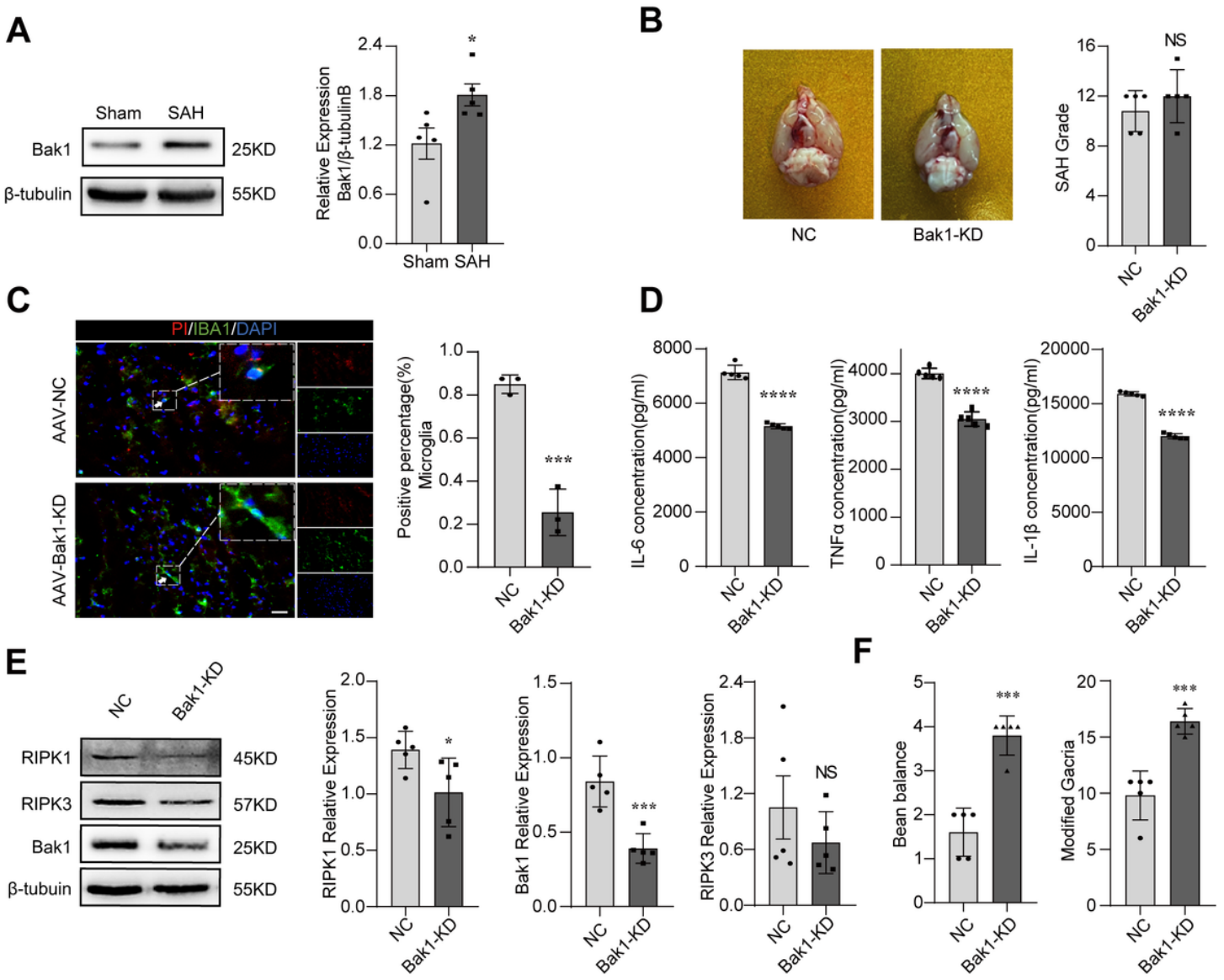

Figure 2

Knockdown microglia Bak1 protein attenuates necroptosis and neuroinflammation. A Bak1 expression in the brain following SAH. the vertical ordinates represent the relative densities of these proteins. n=5 for

each group. *p<0.05 versus the Sham group. **B** Comparison of the degree of SAH in the AAV-NC control group and the AAV-Bak1-KD experimental group, NS=no significant versus the NC group, n=5 in each group. **C** AAV-NC control group and the AAV-Bak1-KD experimental group SAH 24h PI-positive microglia ratio, scale bar =50μm. Magnification ×200. n=3 in each group. ***p<0.001 versus the NC group. **D** ELISA detection the concentration of IL-6, IL-1β, and TNFα in SAH 24h brain tissue of AAV-NC and AAV-Bak1-KD mice, ****p<0.0001 versus the NC group. **E** 24 hours of SAH, the level of Bak1, RIPK1, RIPK3 in AAV-NC group and AAV-Bak1-KD group, the vertical ordinates represent the relative densities of these proteins. *p<0.05, ***p<0.001 versus the Sham group. F Beam Balance and modified Garcia score in AAV-NC and AAV-Bak1-KD mice at SAH 24h. ***p<0.001 versus the NC group.

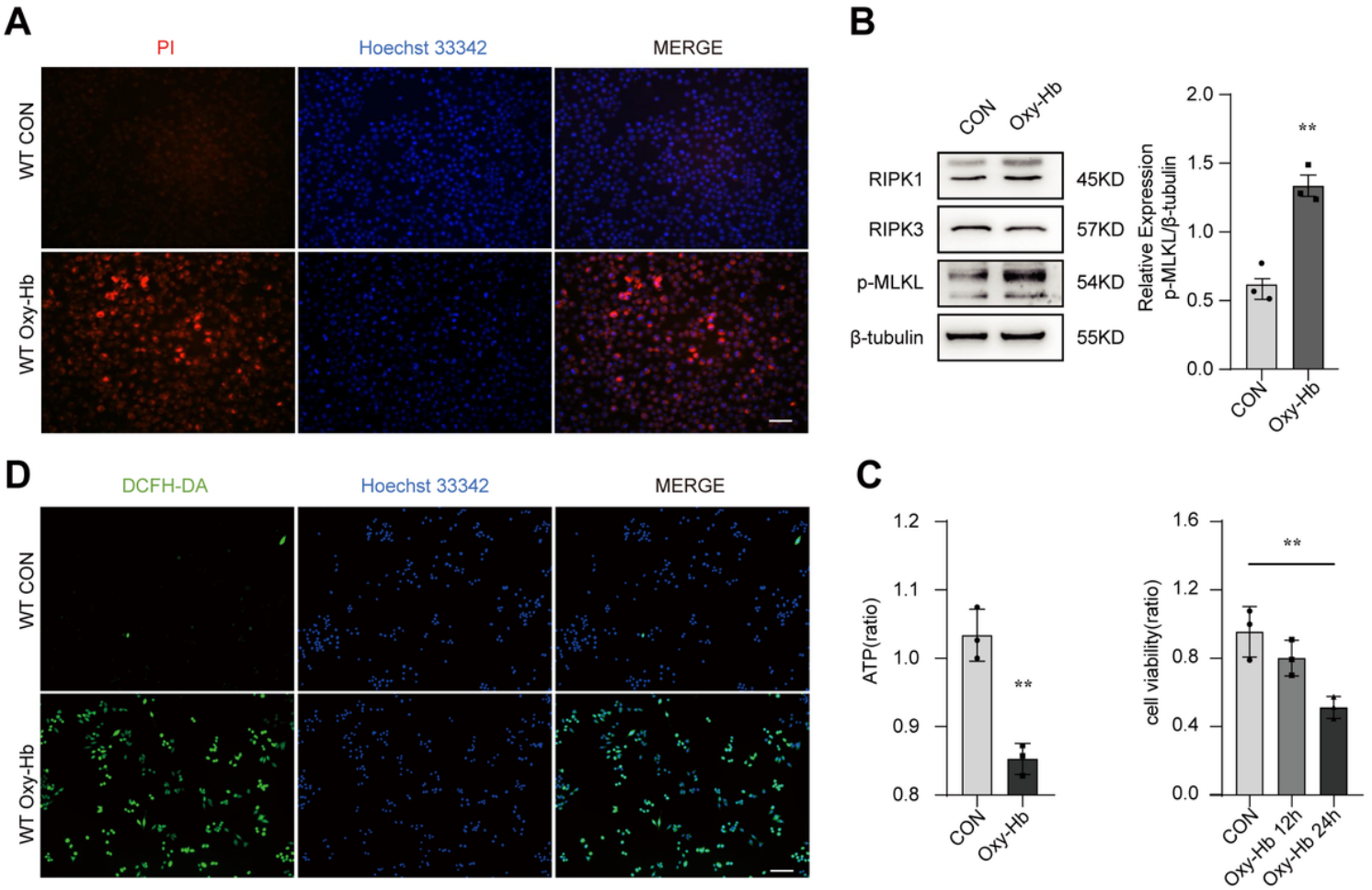

Figure 3

Oxyhemoglobin stimulation induces necroptosis and oxidative stress in microglia. A PI staining to detect microglial cell necrosis after BV2 microglia treated with 10uM oxyhemoglobin, PI (red), nuclei: Hoechst 33342 signal (blue). Scale bar =100μm. Magnification ×100. n =3 in each group. **B** RIPK1, RIPK3, p-MLKL level after BV2 microglia treated with 10uM oxyhemoglobin. The vertical ordinates represent the relative densities of these proteins. **P<0.01 versus the CON group, NS=no significant versus the CON group. **C** ATP was measured using an ATP Assay kit (Beyotime), the intracellular ATP content was measured after 24 h of oxyhemoglobin stimulation, and the results were displayed as a ratio. **P<0.01 versus the CON

group. The cell viability after oxyhemoglobin stimulation was assessed using the CCK8 kit, and results were expressed as the ratio compared with the CON group. **P<0.01 versus the CON group, n=3 in each group. **D** Fluorescence microscopy analysis of DCFH-DA fluorescence after 10uM oxyhemoglobin treated BV2 microglia; nuclei: Hoechst 33342 signal (blue); ROS: DCFH-DA signal (green). Scale bar =100μm. Magnification ×100. n =3 in each group.

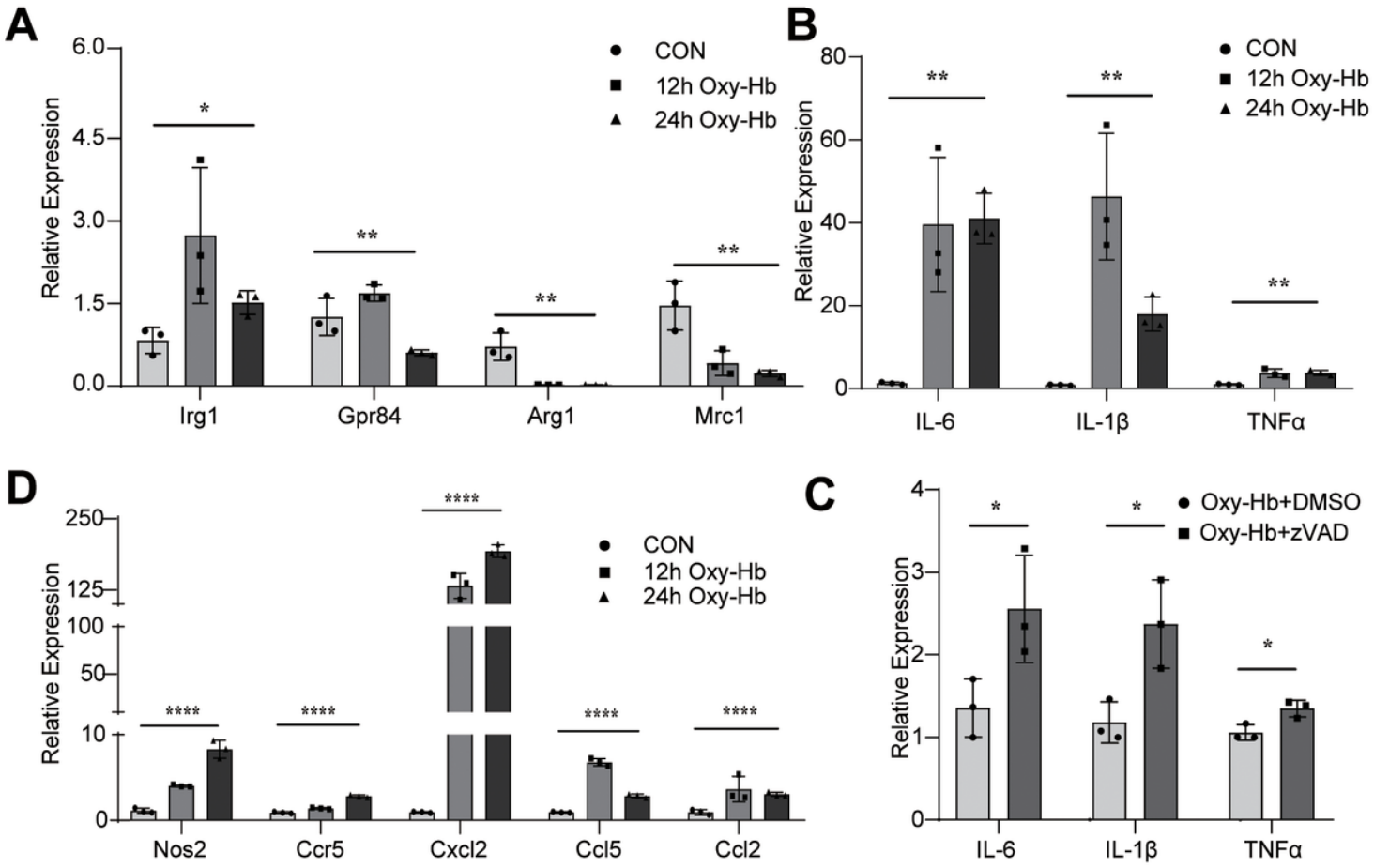

Figure 4

Necroptosis mediates pro-inflammatory phenotype transformation of microglia to exacerbate neuroinflammation. A RT-qPCR detection of Irg1, Gpr84, Arg1, Mrc1 mRNA expression levels in response to 12 h or 24 h of oxyhemoglobin treatment. The RT-qPCR results were normalized using β-action, and the fold change in each gene in the 12 h or 24 h treatment groups was calculated using the $2^{-\Delta\Delta Ct}$ technique in comparison to the untreated control group. Error bars represent mean ± SEM of n=3 independent experiments (biological replicates), and P-values are calculated by one-way ANOVA. *P < 0.05, ** P < 0.01. **B** RT-qPCR detection of IL-6, IL-1β, TNFα mRNA expression levels in response to 12 h or 24 h of oxyhemoglobin treatment. Error bars represent mean ± SEM of n=3 independent experiments (biological replicates). ** P < 0.01. **C** RT-qPCR detection of WT BV2 IL-6, TNFα, IL-1β expression in the presence of oxyhemoglobin combined with zVAD-FMK stimulation. P-values are calculated by unpaired two-tail t-test. *P < 0.05. **D** RT-qPCR detection of Nos2, Ccr5, Cxcl2, Ccl2, Ccl5 mRNA expression levels in response to 12

h or 24 h of oxyhemoglobin treatment. Error bars represent mean ± SEM of n=3 independent experiments (biological replicates). P-values are calculated by one-way ANOVA. **** P < 0.0001.

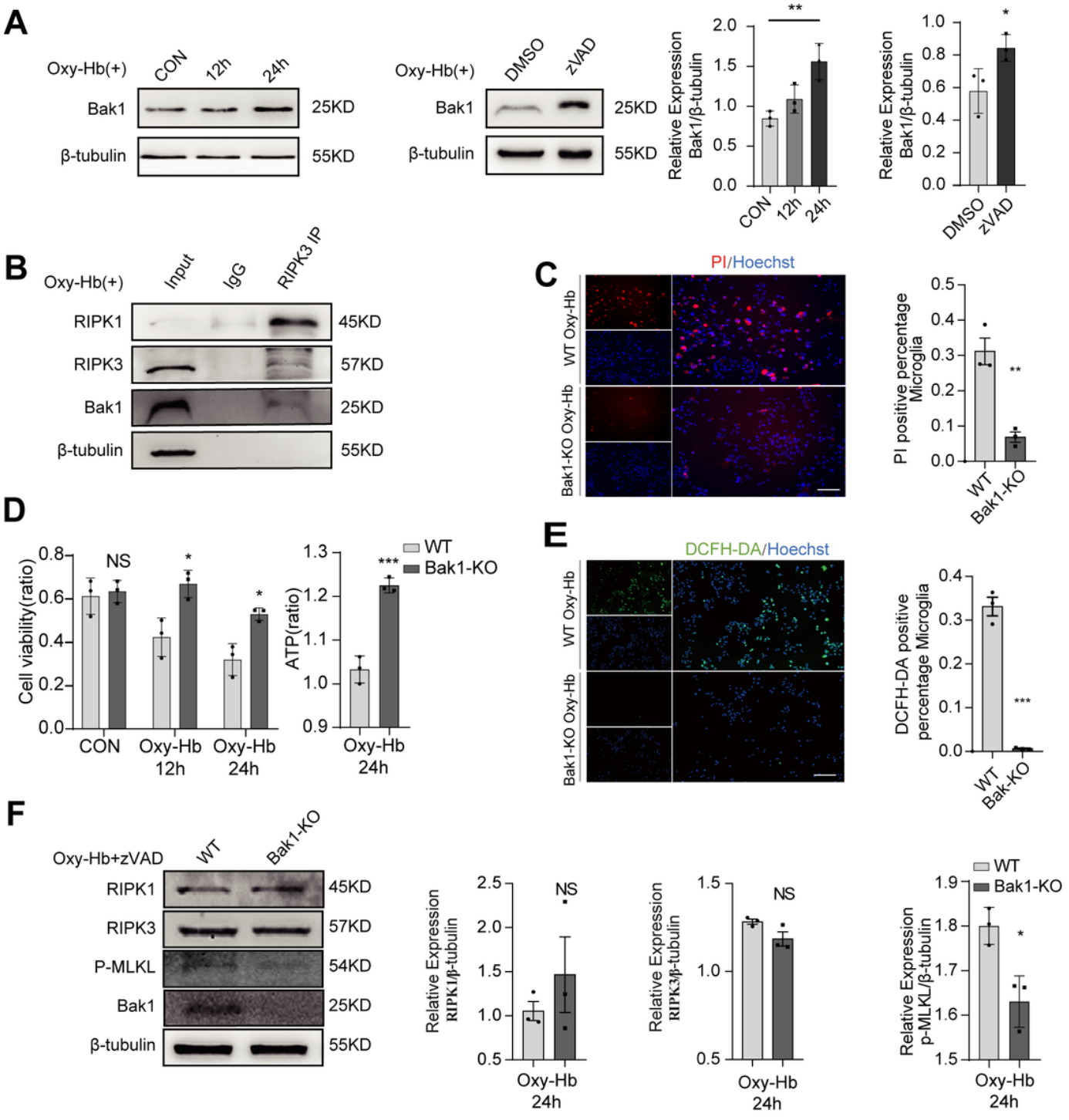

Figure 5

Knockout of Bak1 alleviates microglia necroptosis and oxidative stress. A Bak1 level after BV2 microglia treated with 10uM oxyhemoglobin and 10uM oxyhemoglobin+30uM zVAD-FMK. The vertical ordinates represent the relative densities of the protein. One-way ANOVA was used for comparison between multiple

groups. The unpaired two-tail t-test was used for comparison between the two groups. *P<0.05, **P<0.01. n=3 in each group. **B** Co-immunoprecipitation (Co-IP) of RIPK3 was then subjected to western blot analysis with mouse anti-RIPK1, anti-Bak1. **C** PI staining to detect microglial cell necrosis after WT BV2 and Bak1-KO BV2 treated with 10uM oxyhemoglobin, PI (red), nuclei: Hoechst 33342 signal (blue). Scale bar=50μm. Magnification ×200. The unpaired two-tail t-test was used for comparison between the two groups. **P<0.01. n=3 in each group. **D** ATP was measured using an ATP Assay kit (Beyotime), the intracellular ATP content was measured after 24 h of oxyhemoglobin stimulation, and the results were displayed as a ratio. ***P<0.001, Bak1-KO BV2 versus WT BV2. The cell viability after oxyhemoglobin stimulation was assessed using the CCK8 kit, and results were expressed as the ratio of CCK8. *P<0.05, NS=no significant, Bak1-KO BV2 versus WT BV2, n=3 in each group. **E** Fluorescence microscopy analysis of DCFH-DA fluorescence after 10uM oxyhemoglobin treated WT BV2 and Bak1-KO BV2; nuclei: Hoechst 33342 signal (blue); ROS: DCFH-DA signal (green). Scale bar=50μm. Magnification ×200. The unpaired two-tail t-test was used for comparison between the two groups. ***P<0.001. n=3 in each group. **F** RIPK1, RIPK3, p-MLKL level after WT BV2 and Bak1-KO BV2 treated with 10uM oxyhemoglobin+30uM zVAD-FMK. The vertical ordinates represent the relative densities of these proteins. The unpaired two-tail t-test was used for comparison between the two groups. *P<0.05, NS=no significant. n=3 in each group.

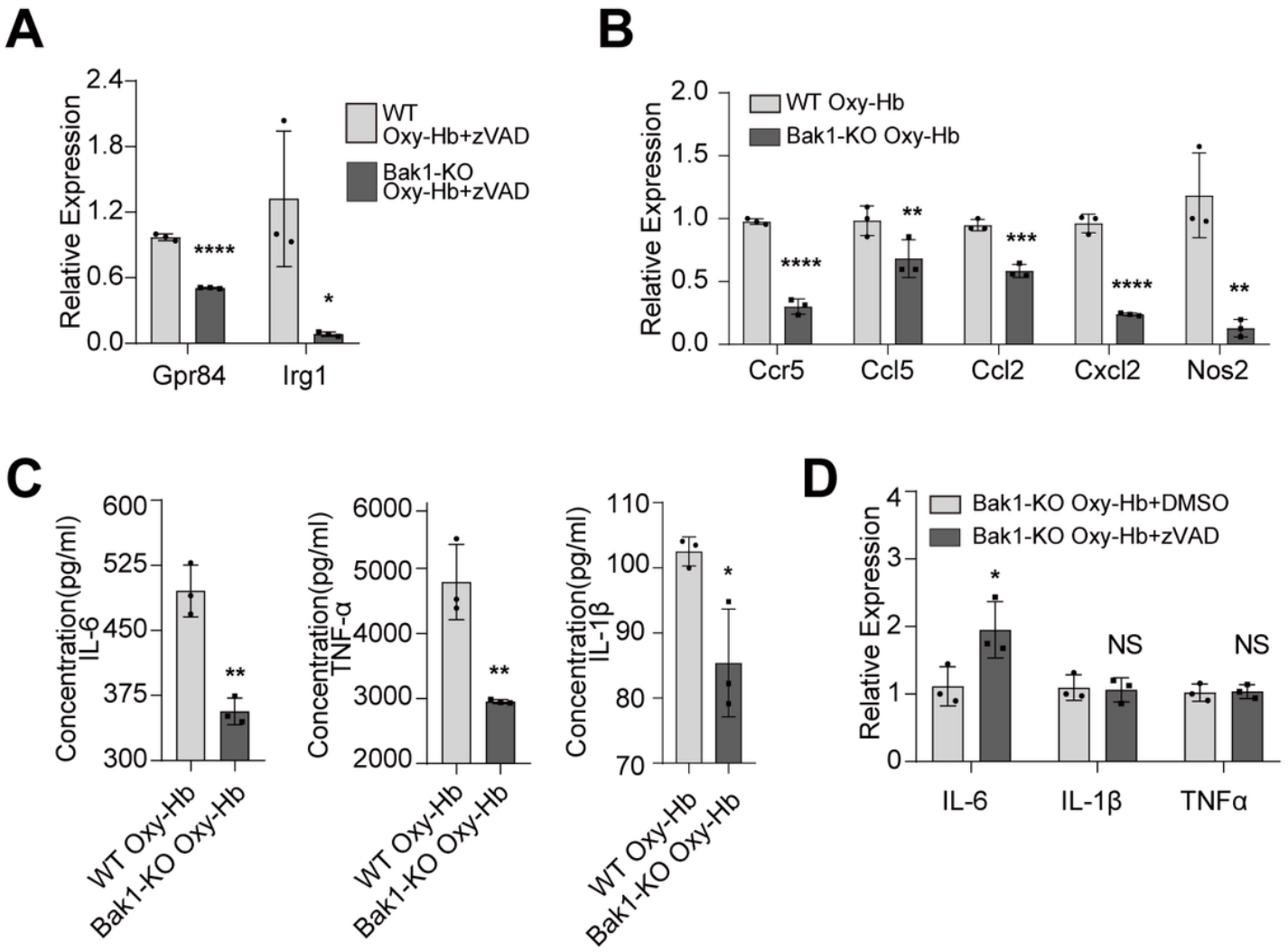

Figure 6

Knockout of microglia Bak1 attenuates pro-inflammatory phenotype transformation and neuroinflammation. A RT-qPCR detection of Irg1, Gpr84 mRNA expression levels in response to 24 h of 10uM oxyhemoglobin+30uM zVAD-FMK treatment with WT BV2 and Bak1-KO BV2. RT-qPCR results were normalized using β-action, and the fold change was calculated with the $2^{-\Delta\Delta Ct}$ method. Error bars represent mean ± SEM of n=3 independent experiments (biological replicates), and P-values are calculated by unpaired two-tail t-test. *P < 0.05, **** P < 0.0001. Bak1-KO BV2 versus WT BV2. **B** RT-qPCR detection of Ccr5, Ccl5, Ccl2, Cxcl2, Nos2 mRNA expression levels in response to 24 h of 10uM oxyhemoglobin treatment with WT BV2 and Bak1-KO BV2, the unpaired two-tail t-test was used for comparison between the two groups. Error bars represent mean ± SEM of n=3. ** P < 0.01, *** P < 0.001, **** P < 0.0001. **C** ELISA detection of the supernatant concentration of IL-6, IL-1β, and TNFα in 10uM oxyhemoglobin treatment with WT BV2 and Bak1-KO BV2, Error bars represent mean ± SEM of n=3. P-values are calculated by unpaired two-tail t-test. *P < 0.05, ** P < 0.01. Bak1-KO BV2 versus WT BV2. **D** RT-qPCR detection of IL-6, IL-1β, and TNFα mRNA expression levels in response to 24 h of 10uM oxyhemoglobin+30uM zVAD-FMK treatment in Bak1-KO BV2. Error bars represent mean ± SEM of n=3 independent experiments (biological replicates), and P-values are calculated by unpaired two-tail t-test. * P < 0.05, *** P < 0.001, **** P < 0.0001. NS=no significance.

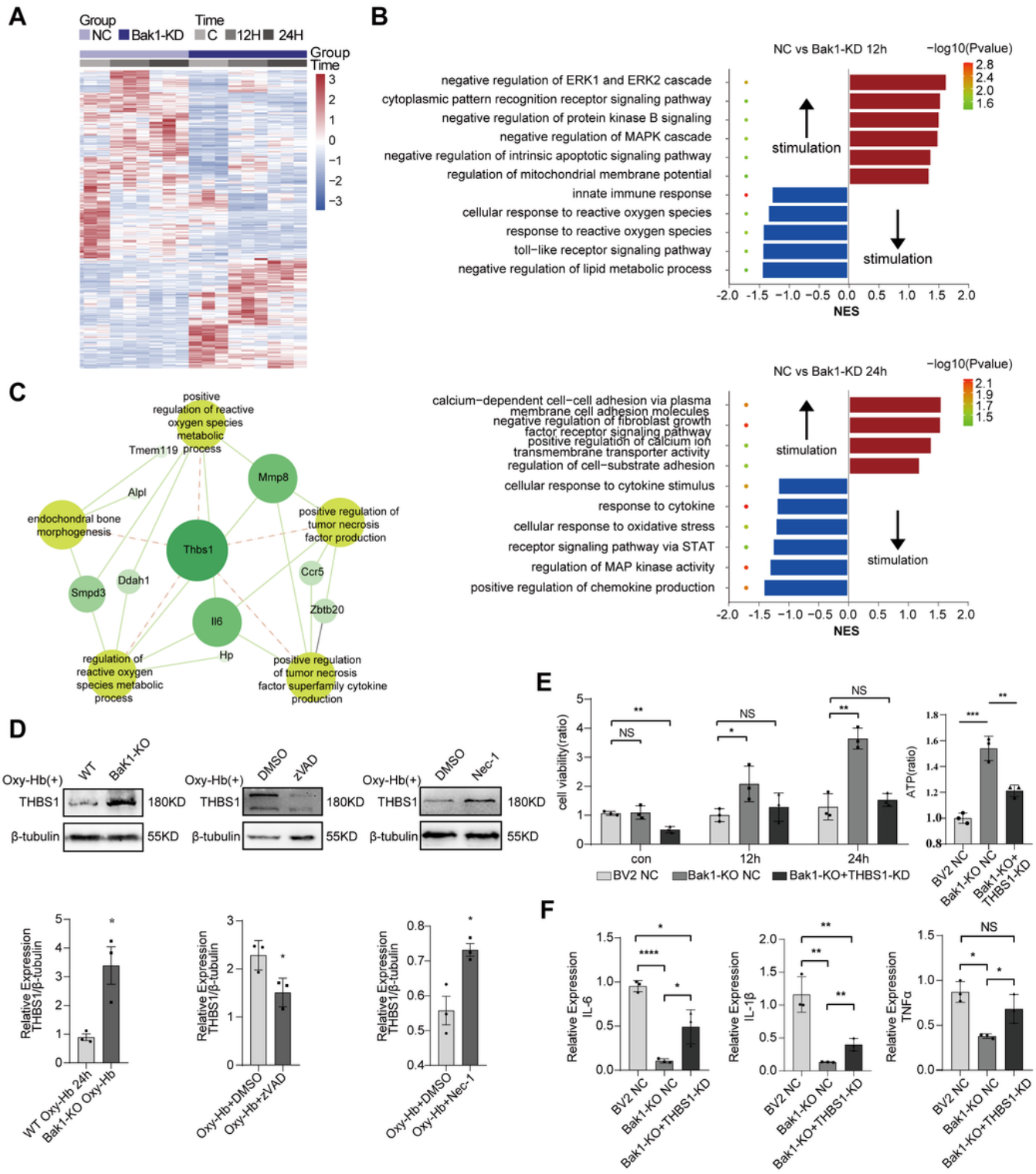

Figure 7

GSEA (Gene set enrichment analysis) analysis of altered GO-BP (Biological Processes) following Bak1 interference and identification of the effect of Bak1 on the high contributing gene *Thbs1*. A DEGs heatmap in microglia exposed to 10μM oxyhemoglobin stimulation for NC and Bak1-KD at CON, 12h, 24h timepoints. K-means splits the significantly altered genes into two clusters. **B** GO-BP of Bak1-KD versus NC using GSEA analysis: The graph shows the 12-hour oxyhemoglobin stimulation and the 24-hour

oxyhemoglobin stimulation. Red indicates up-regulated biological processes, while blue indicates down-regulated. Color bar: -log10 (P-value). NES: normalized enrichment score. **C** THBS1 is involved in the GO biological processes network. The yellow circles represent the altered biological processes caused by Bak1-KD. The green circles represent genes involved in biological processes, and the size of the circles indicates the number of biological processes. **D** THBS1 levels in Bak1-KO, zVAD-FMK, and Nec-1 after 24 hours of oxyhemoglobin stimulation. The vertical ordinates represent the relative densities of the protein. The unpaired two-tail t-test was used for comparison between the two groups. *P<0.05. **E** ATP was measured using an ATP Assay kit (Beyotime), the intracellular ATP content was measured after 24 h of oxyhemoglobin stimulation, and the results were displayed as a ratio. **P<0.01, ***P<0.001, The cell viability after oxyhemoglobin stimulation was assessed using the CCK8 kit, and results were expressed as the ratio of CCK8. *P<0.05, **P<0.01 NS=no significant, versus NC group, n=3 in each group. **F** RT-qPCR detection of IL-6, TNFα, IL-1β mRNA expression levels in response to 24 h of 10uM oxyhemoglobin treatment with BV2 NC, Bak1-KO NC, Bak1-KO+THBS1-KD. P-values are calculated by t-test. ** P < 0.05, *** P < 0.01, **** P < 0.0001. NS=no significant.

Supplementary Files

This is a list of supplementary files associated with this preprint. Click to download.

- Supplementaryfiles.docx